

## STRUCTURAL AND OPTICAL INVESTIGATION OF ZINC OXIDE NANOWALLS AND APPLICATIONS IN pH SENSING

S.P. CHANG\*

*Institute of Microelectronics and Department of Electrical Engineering,  
Center for Micro/Nano Science and Technology, Advanced Optoelectronic  
Technology Center, National Cheng Kung University, Tainan 70101, Taiwan*

Zinc oxide (ZnO) nanowalls were grown under an oxygen atmosphere in a furnace tube using zinc powder. The consequences of increasing the growth time and temperature on the structural, and optical properties of the ZnO nanowalls are discussed. The ZnO nanowalls were grown vertically on glass surfaces, preferentially along the *c*-axis as evident from X-Ray Diffraction (XRD) analysis in every case. The photoluminescence (PL) spectra of the ZnO nanowalls exhibited changes in the emission peaks with increase in growth temperatures. An application of the ZnO nanowalls as a pH sensor is demonstrated. Experimental results revealed that pH sensors fabricated with the ZnO nanowalls demonstrated a change in the current measured through cyclic voltammetry, when the pH was varied from 5 to 11.

(Received April 1, 2014; Accepted May 30, 2014)

*Keywords:* ZnO, nanowalls, tube furnace, pH sensor

### 1. Introduction

Zinc oxide (ZnO) has a relatively large bandgap (3.37 eV) at room temperature in comparison to traditional semiconductors such as silicon (1.12 eV) and germanium (0.66 eV)[1]. Since ZnO can be fabricated into various nanostructures, it has become the material of choice for a wide array of photonic applications such as solar cells, light emitting diodes and gas sensors [2-6]. ZnO has a hexagonal structure along the *c*-axis, and the growth of the one-dimensional (1D) nanowires and nanorods is a relatively simple process as demonstrated previously [7]. In comparison to these, growing two-dimensional (2D) nanostructures is a slightly more complex procedure. However, 2D nanostructures have opened up exciting mechanisms and applications of nanostructures with different dimensionalities. In particular, ZnO nanowalls have attracted much attention because of their large surface areas with potential practical applications as gas sensors [8]. Techniques such as metal organic chemical vapor deposition (MOCVD) are well established for the fabrication of ZnO nanowalls structures [9]. However, this requires a pressurized chamber to grow nanowalls at relatively low temperatures and is moreover a complex and relatively expensive technology often involving the use of toxic metal organic salts and inflammable gases. Therefore, there is a critical need to develop a simple, low-cost and non-toxic process. The fabrication of vertically aligned ZnO nanowalls on a glass substrate using a tube furnace is reported here. In this paper, we report the synthesis of vertically aligned ZnO nanowalls on a glass substrate using thermal evaporation. The surface morphology and structural and optical properties of the nanowalls were investigated using scanning electron microscopy (SEM), X-ray diffraction (XRD), and photoluminescence (PL). Our fabricated ZnO nanowall pH sensors showed good sensitivity.

---

\* Corresponding author: changsp@mail.ncku.edu.tw

## 2. Experimental

The ZnO nanowalls used in this study were grown on 1×1 cm quartz substrate that was successively cleaned with acetone, isopropyl alcohol, and DI water. The ZnO nanowalls were fabricated through a simple, low cost thermal evaporation process inside a tube furnace. The source material was zinc powder placed in an aluminum oxide boat under a flow of oxygen/nitrogen gas. The flow of the oxygen/nitrogen was 10/200 sccm. The distance between the substrate and the powder was approximately 1 cm. The growth times were kept at 5 · 30 · 60 and 120 min for annealing temperature was 450 °C. The other samples of the annealing temperature were 450 °C · 550 °C and 650 °C for growth time was 30min. In order to fabricate the electrode on the ZnO nanowall films, a 100-nm-thick conducting Al layer was deposited on it using a thermal evaporation system. The morphologies of the nanowall films were determined by field-emission scanning electron microscopy (FE-SEM; JSM-7000F), with a beam energy of 10 keV. The optical properties of the ZnO nanowall films were studied by room-temperature photoluminescence measurements with a 325 nm He–Cd laser. The crystallographic properties of the ZnO nanowall films were investigated by X-ray diffraction (XRD) analysis. Raman spectra were obtained using a Near-Field Scanning Optical Microscope imaging system integrated with Raman spectrometer, with 532 nm laser light with Nd:YAG laser as an excitation source. The absorption spectra were measured from UV to visible regions by spectrophotometer. The fabrication process for the ZnO nanowall-based pH sensor is discussed below. Figure 1 illustrates the basic steps involved in the device fabrication. The ZnO nanowalls were deposited on quartz substrate by furnace tube, and then the Al electrode was deposited on ZnO nanowalls. The experimental setup for the pH sensing system is shown in figure 2. To measure the sensing performance of the fabricated pH sensors, the Pt counter electrode, Ag/AgCl reference electrode and ZnO nanowall- film working electrodes were dipped into a buffer solution (pH varied from 5 to 11), which depends on the concentration of the H<sup>+</sup> ions of the detection solution. In order to achieve the desired pH value, solutions of hydrochloric acid and sodium hydroxide were used. The sensing response of the pH sensor was measured using a CH Instrument Model 600D analyzer.

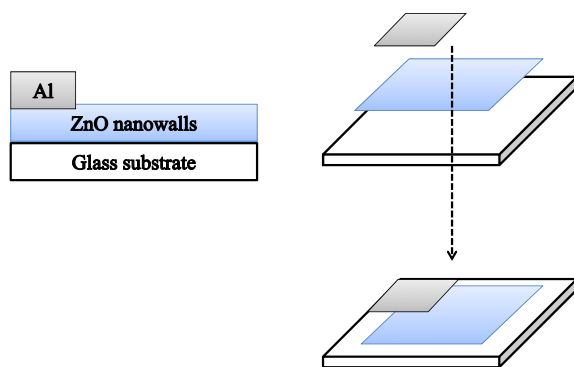
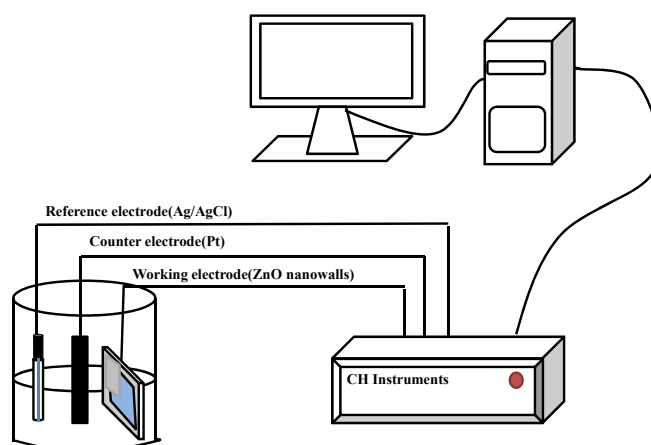


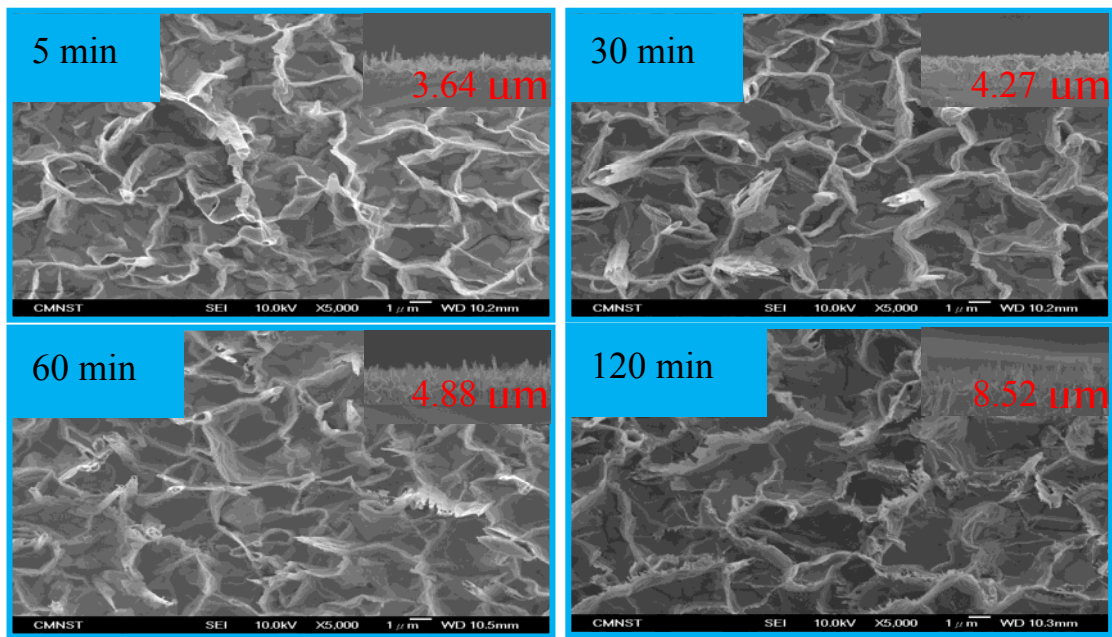
Fig. 1 Illustration of the ZnO nanowall pH sensors fabrication.



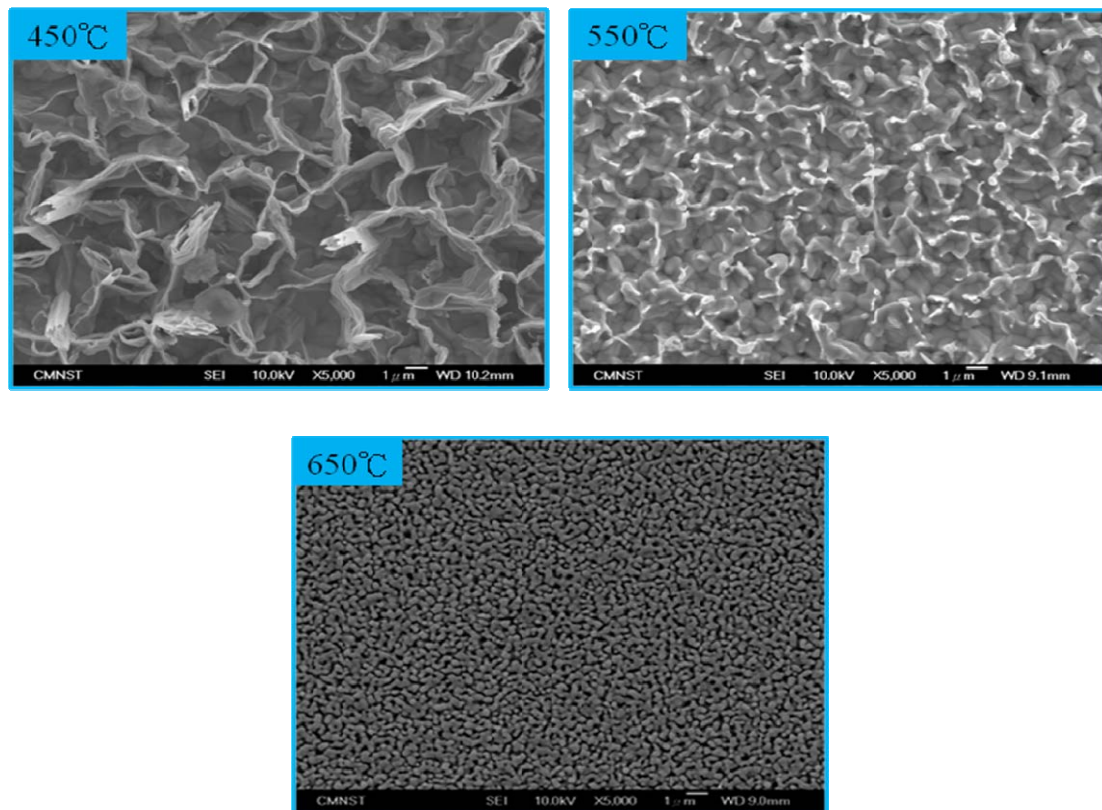
*Fig. 2 Experimental setup of the ZnO nanowall pH sensor.*

### 3. Results and discussion

Figure 3(a) shows the scanning electron microscopy (SEM) images of the ZnO nanowalls grown at 450 °C. The top view of the SEM image indicates that most of the nanowall structures are oriented perpendicular to the substrate, although a small percentage are oriented at a slight angle with the substrate. In addition, there are some tubular ZnO structures formed with interconnected nanowalls. The inset shows the cross-section of the sample which indicates that there is an additional layer between the substrate and nanowalls, possibly attributed to the quartz don't have any lattice and ZnO buffer layers have grown on the substrate in order to form the ZnO nanowalls. As expected, with an increase in the growth time, the height of ZnO nanowalls also increases. It was seen that the approximately heights of the nanowalls grown for 5, 30, 60, and 120 min was 3.64, 4.27, 4.88, and 8.52  $\mu\text{m}$ , respectively. Figure 3(b) shows the scanning electron microscopy (SEM) images of the ZnO grown in different temperatures. We can discover the nano structure of ZnO become dots with the temperature raise to 650°C.



(a)



(b)

Fig. 3(a),(b) SEM images of ZnO nanowalls prepared at different annealing temperatures and growth times.

Figure 4 shows the Raman spectra of the ZnO sample obtained at three different temperatures (450, 550, and 650°C). The strongest peak for ZnO observed at 438  $\text{cm}^{-1}$ , which corresponds to the E2 High nonpolar phonon mode, associated with oxygen. There are no obvious differences in the position of the peaks between each sample annealed at the three different temperatures. These results are also consistent with previous Raman studies that confirm the existence of ZnO nanocrystals in the wurtzite phase. Figure 5 shows the XRD  $2\theta$  diffraction spectra of the ZnO nanowall film, which shows a strong peak correspondence to the ZnO(002) plane which indicates that the ZnO nanowall film are grown vertically on the glass, preferentially along the c -axis. However, with different annealing time, we can discover the FWHM changed. Thus, it can be stated that the annealing time plays an important role of ZnO preferential orientation. There is also a weak (101) peak that indicates that a few c -axis oriented ZnO nanowalls are not perpendicular to the substrate. This result indicates that the ZnO nanowall-film fabricated by the low cost tube furnace approach exhibits high crystallinity and a pure hexagonal structure.

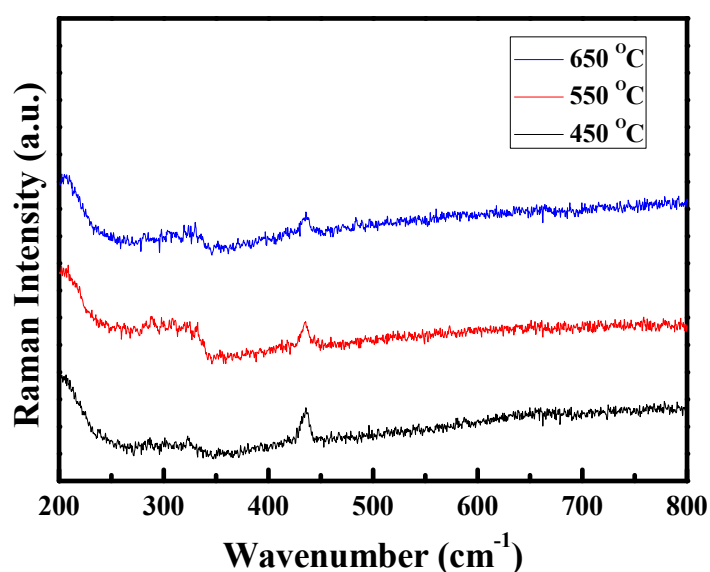


Fig. 4 Raman spectra of ZnO nanowalls annealed at 450, 550, and 650°C.

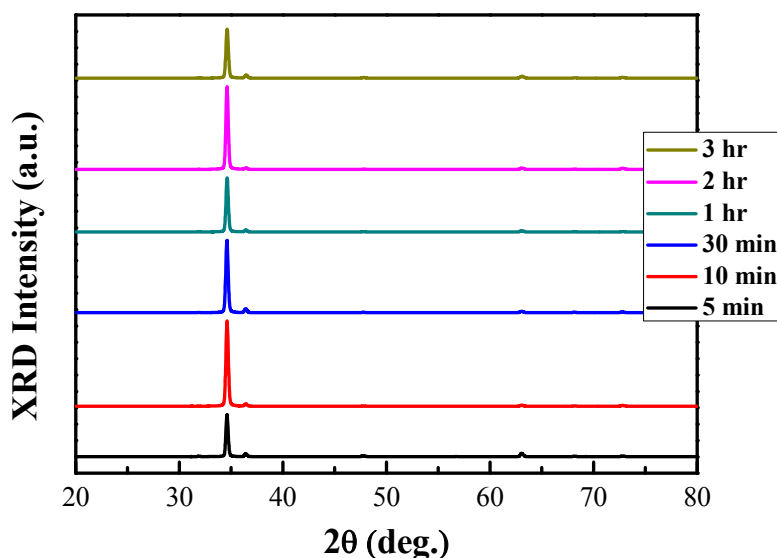
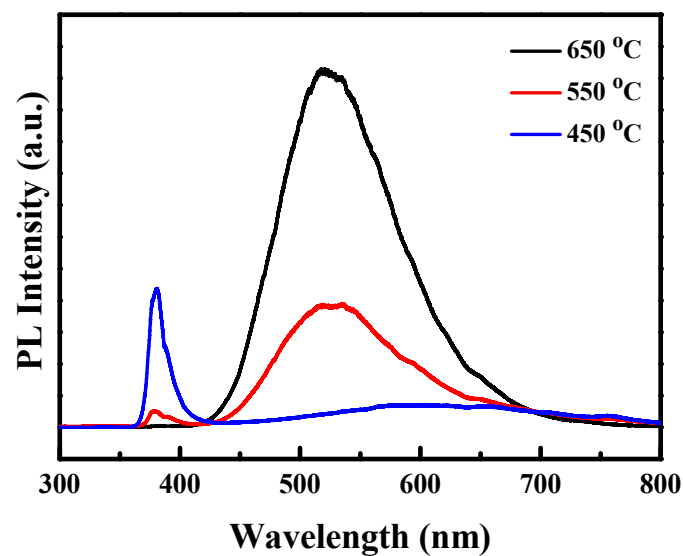
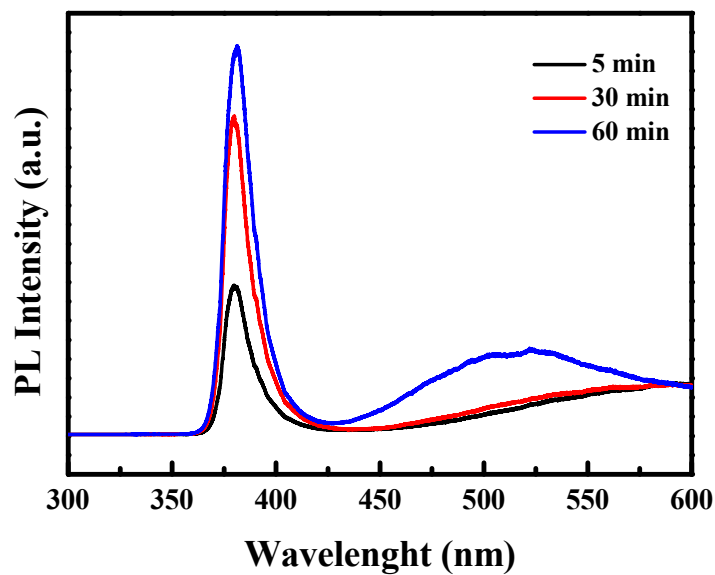


Fig. 5 XRD pattern of the ZnO nanowalls as a function of annealing time.

Figure 6(a) shows the PL spectra of the structures grown at different temperatures. While all the peaks can be attributed from ZnO nanowalls, the UV emission peak at 450 °C can be attributed to the near-band edge (NBE) that is closer to the bandgap of bulk ZnO (3.36 eV). ZnO nanowalls grown at 550 °C exhibits a weak UV emission peak and a strong yellow-green defect emission peak. The green-yellow emission is associated with either the surface state or oxygen vacancy (Vo) and zinc interstitials (Zni). At 650 °C, the emission peaks of the nanowalls are completely shifted towards the yellow-green defect emission peak. In all cases, annealing above 450 °C produces a red shift in the defect emission peak. The time-dependence PL spectra from ZnO nanowalls grown for 5 to 60 min have been measured as seen in figure 6(b) and the emission peaks are similar for the structures grown at the different temperatures. With shorter growth times, the full width at half maximum (FWHM) is larger than that of the longer growth times which can be attributed to the quality of crystallization as well as the increased annealing time.



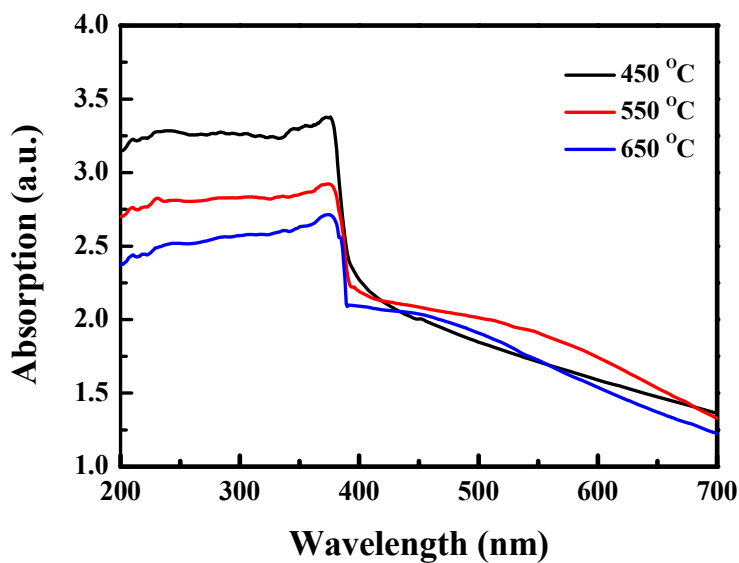
(a)



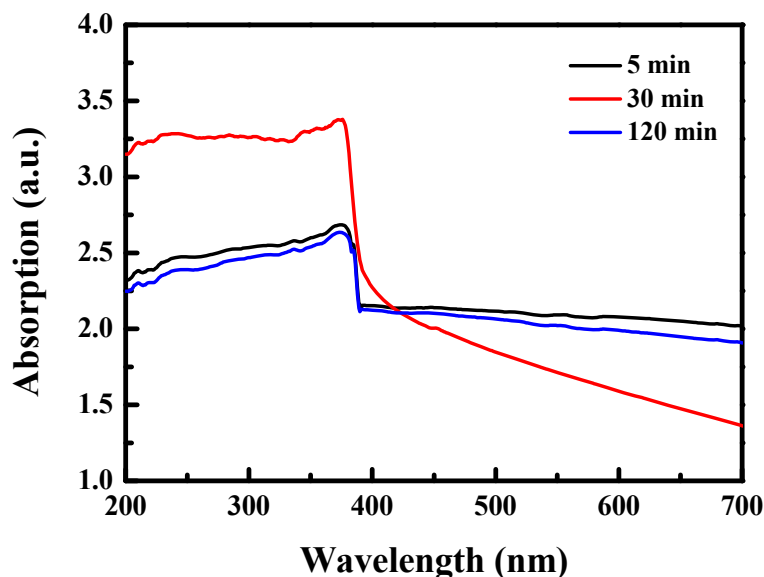
(b)

Fig. 6(a),(b) PL spectra of the ZnO nanowalls at different annealing temperatures and growth times.

The absorption coefficient ( $\alpha$ ) is shown in figure 7(a), as a function of the wavelength, for three films deposited at 450, 550, and 650 °C. In all three cases, the optical absorption exhibits a sharp decrease at 400 nm. The sharpness of this transition allows us to determine a value of the absorption wavelength by extrapolating the linear part of the curve down to the wavelength axis. With an increase in the growth temperature, a negligible difference between the absorption wavelengths is observed. The absorption wavelength for the film deposited at 5, 30, and 120 min was also evaluated at 400 nm and showed in figure 7(b). It is seen that the absorption ratio of UV emission to that of the visible band is higher for the films deposited at 30 min. This increase in the absorption ratio is a result of the enhancement in crystalline quality of the films deposited.



(a)



(b)

Fig. 7(a),(b) Absorption spectra of the ZnO nanowalls at different annealing temperatures and times.

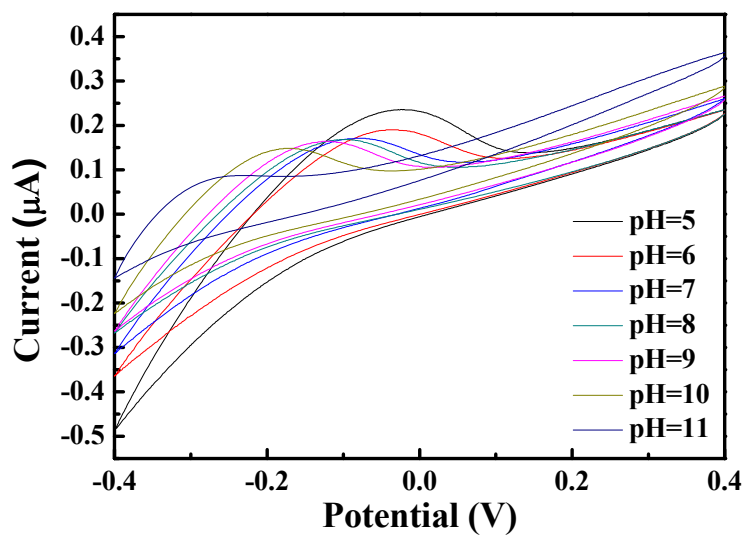


Fig. 8 Cyclic voltammety curves of ZnO nanowalls at different pH value.

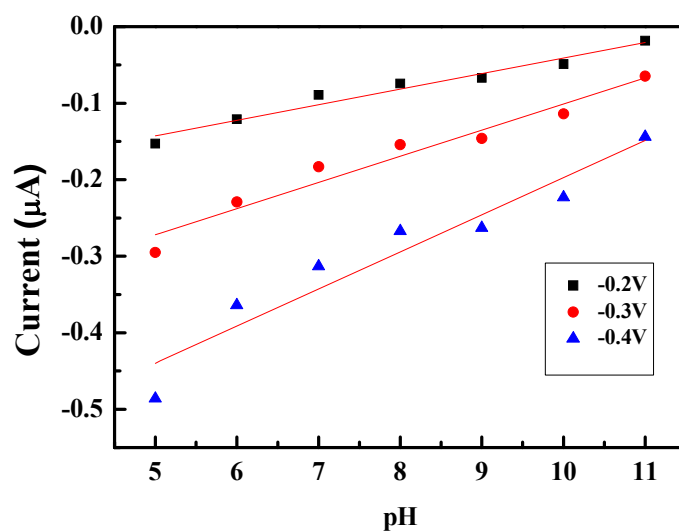


Fig. 9 Plot of cyclic voltammety currents as a function of pH values at -0.2, -0.3, and -0.4 V.

Table 1 Sensitivity and R-square of ZnO nanowalls

Potential (V)	-0.2 V	-0.3 V	-0.4 V
R-Square	0.95714	0.94554	0.90763
Sensitivity( $\mu\text{A}/\text{pH}$ )	0.02036	0.03421	0.0485

The pH sensor was characterized using cyclic voltammetry to measure the current response of ZnO nanowalls as shown in figure 8. It can be seen that the cyclic voltammetry curve shifted as a function of the pH value. With a decrease in the pH value, the current response is higher at a potential (V) of -0.4 V. On the other hand, the pH value increase resulted in a lower current response. Figure 9 shows the current response as a function of the pH value at potentials -0.2, -0.3, and -0.4 V. The sensitivity defined as the current response current to a specific pH value is calculated from the linear relationship between the response currents and the pH value. Based on the experimental results, the sensitivity were calculated and listed in Table 1. R squared indicated how well data points fit the linear line. The sensitivity of the pH sensor with ZnO nanowalls at three different potentials was calculated to be 0.02036, 0.03421, and 0.0485  $\mu\text{A}/\text{pH}$ , respectively. It was determined that the ZnO nanowalls exhibit the greatest sensitivity at a potential value of -0.4 V. Even ZnO nanowalls may be removed by acid or alkaline, it still can be applied on the single-use pH sensor for its great sensitivity and accuracy.

#### 4. Conclusions

In summary, high-quality ZnO nanowalls have been synthesized on glass substrates by a simple method. The scanning electron microscopy (SEM) images showed that nanowalls preferred a orientation perpendicular to the substrate, and the XRD pattern indicated that nanowalls are oriented in the (002) direction. The PL spectra shows a yellow-green defect emission, which would arise when increasing annealing temperatures and times. The absorption wavelength was evaluated at 400 nm for all cases. Cyclic voltammetry currents have strong pH dependence, and the highest sensitivity was 0.0485  $\mu\text{A}/\text{pH}$  at -0.4 V. Thus, ZnO nanowalls thus fabricated are promising structures in pH sensing applications.

#### Acknowledgements

This work was supported by the National Science Council under the contract number NSC 100-2221-E-006-168. This work was also supported in part by the Center for Frontier Materials and Micro/Nano Science and Technology, National Cheng Kung University, Taiwan. The authors would also like to acknowledge the support by the Advanced Optoelectronic Technology Center, National Cheng Kung University, under projects from the Ministry of Education.

#### References

- [1] K. Vanheusden, C. H. Seager, W. L. Warren, D. R. Tallant, J. A. Voigt, *Appl. Phys. Lett.* **68**, 403 (1996)
- [2] W. Han, Y. Zhou, Y. Zhang, C. Y. Chen, L. Lin, X. Wang, S. Wang, Z. L. Wang, *ACS Nano* **6**, 3760 (2012)
- [3] S. K. Mehta, K. Singh, A. Umar, G. R. Chaudhary, S. Singh, *Electrochim. Acta* **69**, 128 (2012)
- [4] S. P. Chang, K. J. Chen, *J. Nanomater.* **2012**, 602398 (2012)
- [5] S. P. Chang, T. H. Chang, *J. Nanomater.* **2011**, 903176 (2011)
- [6] S.P Chang, C.W. Li, K. J. Chen, S.J. Chang, C.L. Hsu, T.J. Hsueh, H.T. Hsueh, *Sci. Adv. Mater.* **4**, 1174 (2012)
- [7] Z. L. Wang, X. Y. Kong, and J. M. Zuo, *Phys. Rev. Lett.* **91**, 185502 (2003)
- [8] S. W. Kim, H. K. Park, M. S. Yi, N. M. Park, J. H. Park, S. H. Kim, S. L. Maeng, C. J. Choi, S. E. Moon, *Appl. Phys. Lett.* **90**, 033107 (2007)
- [9] S. W. Kim, S. Fujita, M. S. Yi, D. H. Yoon, *Appl. Phys. Lett.* **88**, 253114 (2006)